Reinhold Kleiner and Huabing Wang

12 $Bi_2Sr_2CaCu_2O_8$ intrinsic Josephson junction stacks as emitters of terahertz radiation

12.1 Introduction

One of the interesting properties of Josephson junctions is their ability to emit electromagnetic radiation, with emission frequencies f_e that are tunable via the voltage drop V_J across the junction. More precisely, the emission frequency obeys the relation $f_e = V_J/\Phi_0$, where $\Phi_0 = h/2e$ is the flux quantum and $\Phi_0^{-1} = 483.6\,\mathrm{GHz/mV}$. In principle, f_e can reach values of up to $2\Delta/h$, where Δ is the energy gap of the superconductor. For higher frequencies quasiparticle excitations in the superconducting electrodes of the Josephson junctions damp the Josephson oscillations and the associated emission of electromagnetic waves. For example, for niobium the gap limit is about 750 GHz and Nb-based Josephson junctions have indeed been operated as local oscillators up to such frequencies [1]. In general, however, single Josephson junctions are not very good oscillators. The output power is low (often nanowatts or less) and the linewidth of radiation is large. Also, the impedance of typical junctions is very low and hard to match to an environment. These problems can be solved at least in principle by using arrays of phase-synchronized Josephson junctions [2–5]. Planar arrays of Nb-based Josephson junctions have been synchronized to have an output power of about 65 μW at frequencies around 134 GHz and about 2 μW at 320 GHz [5]. A particularly interesting system are so-called intrinsic Josephson junctions (IJJs) which naturally form in some of the strongly anisotropic and layered cuprate superconductors [6]. In $Bi_2Sr_2CaCu_2O_8$ (Bi-2212) such an IJJ has a thickness of 1.5 nm and a single crystal of, say, 1 μm thickness can be viewed as a vertical stack of ~700 IJJs. IJJs have been shown to have low damping, which is important for high-frequency generation. Thanks to the large energy gap of cuprates weakly damped Josephson oscillations are, at least in principle, possible at frequencies up to the 10 THz range. Particularly the frequency regime between 0.5 THz and a few THz is very interesting, because there is still a lack of compact solid state sources for electromagnetic radiation [7, 8]. In the decade after the discovery of the intrinsic Josephson effect stacks with a number of IJJs typically ranging from 1 to some 10 have been investigated, with lateral sizes ranging from ~ 50 μm down to the sub-μm range. High-frequency properties as well as microscopic questions like the degree of coherence in interlayer transport or the formation

Reinhold Kleiner, Physikalisches Institut, Universität Tübingen, Auf der Morgenstelle 14, D-72076 Tübingen

Huabing Wang, National Institute for Materials Science, Tsukuba 3050047, Japan and Research Institute of Superconductor Electronics, Nanjing University, Nanjing 210093, China

DOI 10.1515/9783110456806-013,

of vortex structures were the main scientific targets. For reviews on these activities, see [9–11]. In view of THz emission for this type of structure an in-phase oscillation of the Josephson currents across all junctions in a stack is hard, if not impossible to achieve. The situation changed in 2007 when the observation of coherent (sub)THz emission in IJJ stacks was reported [12]. Here, stacks with lateral sizes on the 100 μm scale have been used, with a total number of junctions of about 700. This finding triggered a large amount of experimental and theoretical activities and a lot of progress has been made. While in [12] the maximum integrated emission power was around 0.5 μW and the maximum emission frequency was around 0.8 THz, in recent works the emission power of single IJJ stacks increased to the 100 μW range and the maximum emission frequencies to more than 2 THz. Reviews on the early stages of this research are [11, 13]. A more recent one is [14].

The remainder of this chapter is organized as follows. In Sections 12.2 and 12.3 we introduce some general concepts of the intrinsic Josephson effect and some theoretical considerations. These sections are mainly based on results obtained for the "small" stacks. The final Section 12.4 addresses properties of the "large" stacks, including electromagnetic and thermal properties.

12.2 General properties of intrinsic Josephson junctions

In Bi-2212, CuO_2 double layers of a total thickness of about $d_s = 0.3$ nm are separated by SrO and BiO layers, cf. Figure 12.1a. Cooper pairing is restricted to the CuO_2 layers. The basic picture for the intrinsic Josephson effect arises from the notion that for c-axis transport between adjacent CuO_2 layers the SrO and BiO sheets form a tunnel barrier for both quasiparticle and Cooper pair transport. A suitable patterned Bi-2212 single crystal naturally forms a stack of IJJs, each having a thickness $s = 1.5$ nm. It has turned out that the current voltage characteristics (IVCs) of such junctions are tunneling-like and strongly hysteretic. This is shown in Figure 12.1b for a single IJJ patterned from a $Bi_2Sr_2Ca_2Cu_3O_{10}$ (Bi-2223) thin film [17]. As a result, the c-axis IVCs of a stack of many IJJs have a relatively complex structure arising from the bistability of the IVCs of individual junctions in a certain current range. Figure 12.1c shows an early measurement of an IVC, as measured for a $(30\,\mu m)^2$ wide and 1 μm thick single crystal [16]. The crystal quality was not perfect so that different IJJs in the stack had slightly different properties. Ramping up the bias current from zero all IJJs are in their zero-voltage state up to $I \approx 12$ mA, when some of the junctions switch to their resistive states. By ramping up and down the bias current repeatedly a large amount of branches can be traced out differing by the number of junctions in the resistive state. In Figure 12.1c one observes six branches that are approximately equally spaced. Here, between one and six IJJs have switched to their resistive state while the other IJJs are still in the zero voltage state. One also notes some nearby branches where the total number of IJJs in the resistive state is the same but realized by different individual IJJs. Another example of

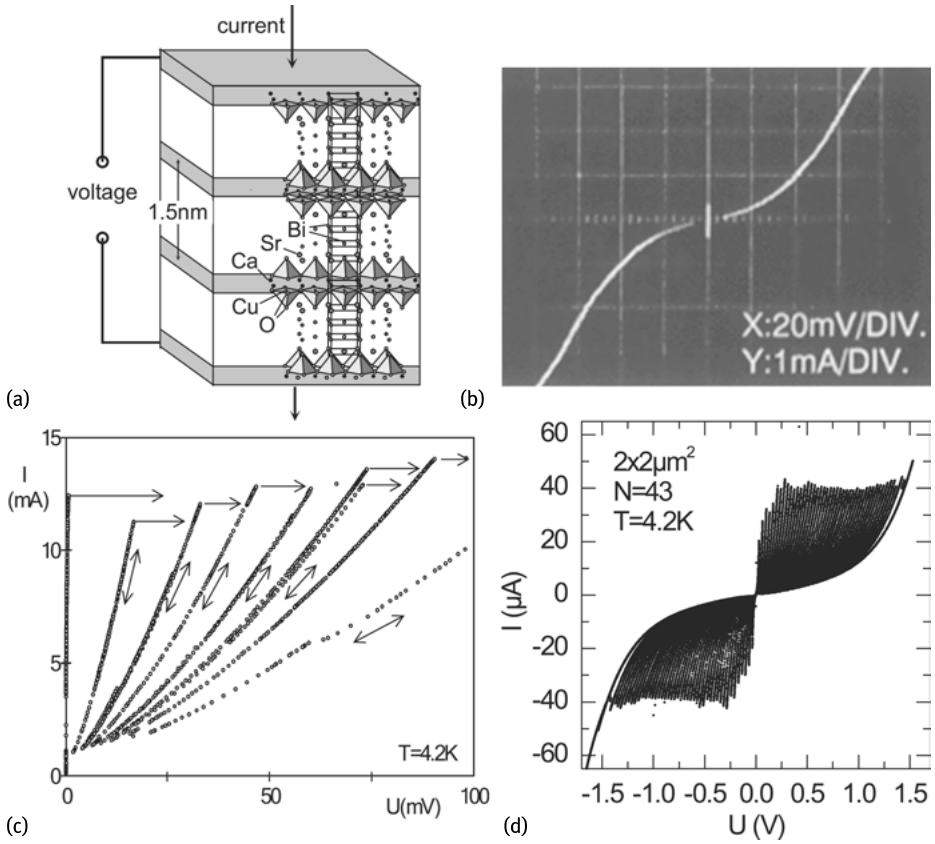

Fig. 12.1: (a) Superposition of the Bi-2212 crystal structure and the model underlying the intrinsic Josephson effect. Superconducting and insulating layers are indicated by, respectively, gray and white sheets. (b) IVC of a single IJJ patterned from a Bi-2223 thin film (after [15]). (c) Section of an IVC as measured for a 30 μm^2 large Bi-2212 single crystal (after [16]). (d) IVC of a 43-junction stack patterned as a 2×2 μm^2 wide mesa structure on top of a Bi-2212 single crystal.

a 43 junction stack is shown in Figure 12.1d. This stack was patterned as a 2×2 μm^2 wide mesa structure on top of a Bi-2212 single crystal.

Besides the Bi-based cuprates (Bi-2212, Bi-2223, Bi-2201) [6, 17, 18] many other layered superconductors exhibit an intrinsic Josephson effect. This includes in the cuprate family Tl- and Hg-based compounds [16, 19, 20], strongly underdoped $YBa_2Cu_3O_{7-x}$ [21], electron-doped cuprates [22] and also the ruthenocuprates [23]. There are also organic compounds like κ-$(BEDT{-}TTF)_2Cu(NCS)_2$ [24] and members of the iron pnictide family [25].

Although IJJ stacks have been fabricated from thin films [17, 20, 21, 26], Bi-2212 single crystals remain the workhorse for most investigations and applications. Reliable fabrication techniques to pattern suitably sized and contacted IJJ stacks have been

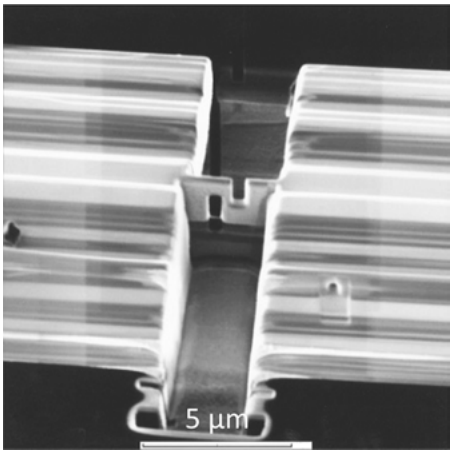

Fig. 12.2: Z-shaped all-superconducting Bi-2212 structure patterned by focused ion beam milling from a Bi-2212 single crystal. The center of the Z-shaped part forms the active IJJ stack. After [21].

developed. While in early experiments the ab-faces of small-sized crystals have been simply covered with gold and contacted with Au rods, in subsequent experiments mesa structures, patterned on top of single crystals and contacted by Au or Ag layers, have been used for investigations. This technique is still widely used. Also, focused ion beam techniques have been applied for patterning Z-shaped structures from the interior of single crystals or thin films [21], cf. Figure 12.2. A special patterning technique for Bi-2212 single crystal arises from the fact that these crystals can be cleaved easily, allowing for a double-sided fabrication method [28]. Here, a single crystal is mounted to a first substrate and patterned from the top. Then a second substrate is glued on this patterned surface, the first substrate is removed and a second patterning step is used to structure the surface which in the first step was glued to substrate 1. The various steps and a resulting array of stacks embedded in a planar bow-tie antenna are shown in Figure 12.3. In a similar fashion it is also possible to create a stand-alone Bi-2212 stack which is embedded between Au layers [29].

In the IVC of Figure 12.1c typically a maximum voltage around 12 mV per IJJ could be obtained which, according to the Josephson relations, corresponds to an oscillation frequency of about 6 THz. Depending on the doping state of the crystal and on the compound used this maximum voltage per junction can even be higher, reaching values of the order of 30 mV, corresponding to a Josephson frequency of 15 THz. The smallest voltages that can be applied before the switch-back to the zero-voltage state occurs are of the order of 0.5 mV (250 GHz). Thus, a suitably patterned stack of IJJs can at least in principle act as a broadly tunable source for THz radiation. Indeed, indirect evidence has been found that inside the stack the Josephson oscillations can excite phonons [26, 30, 31]. The interaction of the Josephson system and the phonons leads to subgap-structures on the IVCs visible in Figure 12.4. Some of the structures are marked V_n^m in the graph, the lower index indicating the branch number and the upper number indexing the subgap structure on a given branch of the IVC. It in fact

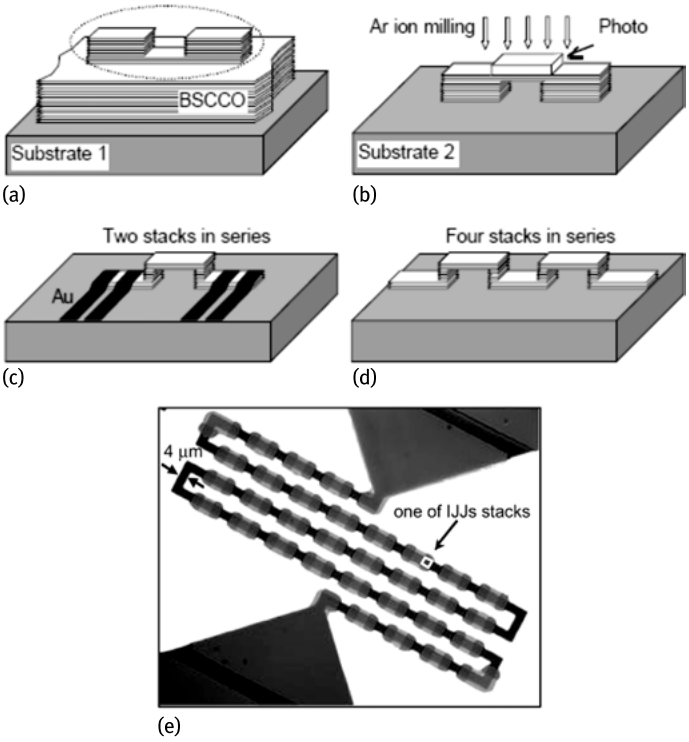

Fig. 12.3: Series array of 64 all-superconducting IJJ stacks, patterned using the double-sided fabrication method [27].

turns out that the subgap features on branch numbers > 1 are just replicas of the structures on the first branch, their multiplicity explainable by the number of combinations that are allowed to have the n resistive IJJs on one of the voltage states created by the sub-branches. More importantly, the structures were visible up to 7.9 mV (3.8 THz) on the first branch of the Bi-2212 IVC, and up to 9.7 mV (4.7 THz) for a Tl-2223 sample. Thus, the subgap features demonstrate that at least up to these frequencies there are significant ac electric fields in the stack. As a new feature compared to Figure 12.1, Figure 12.4a shows that for large currents and for high branch numbers the IVC exhibits back-bending. The effect is due to Joule heating and the facts that (i) the Bi-2212 c-axis resistance increases with decreasing bath temperature and (ii) the thermal conductivity is low. Qualitatively, with increasing input power the mesa heats up and its resistance decreases. At some input power the voltage across the stack reaches a maximum and then decreases with increasing current. A quantitative description will be given in Section 12.4. Here we only mention that one faces a temperature rise of several Kelvin per mW of input power, the precise value depending on details of the geometry used. The existence of Josephson oscillations in the THz range has also been shown

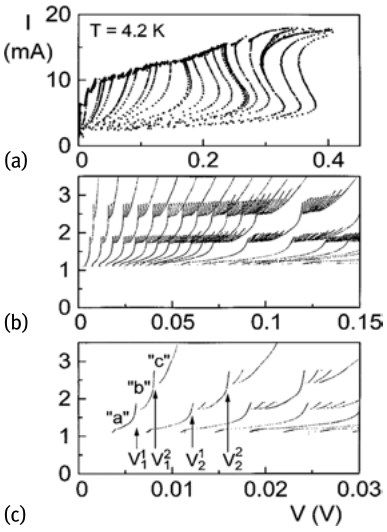

Fig. 12.4: Subgap structures on the IVC of a Bi-2212 stack appearing via coupling of the ac Josephson oscillations to phonons. (a) shows the full-scale IVC (not all branches traced out), (b) and (c) are zooms for expanded current and voltage scales. From [26].

in absorption when applying external radiation to an IJJ stack. For frequencies in the THz regime Shapiro steps from intrinsic junction stacks have been observed by Rother et al. [33, 34] by irradiating a mesa structure incorporated into a bow-tie or logarithmic periodic antenna with a far infrared laser. In these early experiments the power coupled into the system was relatively low; still, however, the first Shapiro step could be detected up to about 2.5 THz. By using the double-sided fabrication technique Wang et al. [27, 28, 32] integrated an IJJ stack with a superconducting antenna structure, as shown in Figure 12.5. The figure also shows the response of the 17-junction mesa to a 1.6 THz far infrared field. Large Shapiro steps appear on all resistive branches of the current voltage characteristic. Shapiro steps under 760 GHz irradiation have also been detected for the 64-stack array shown in Figure 12.3, and for even larger arrays consisting of up to 256 stacks containing in total more than 11000 IJJs in series [27].

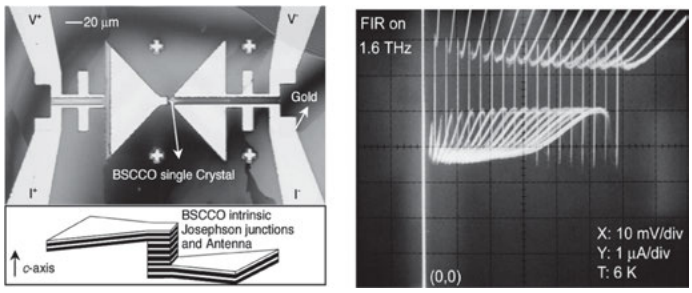

Fig. 12.5: $Bi_2Sr_2CaCu_2O_8$ single crystal patterned into a 17-junction mesa structure integrated with a bow-tie antenna structure (left) together with a current voltage characteristic at 6 K under far infrared irradiation at 1.6 THz (from [32]).

In [28] it has also been shown that, when irradiating the sample both with 760 GHz and an 18 GHz microwave field, up to the $90th$ harmonic of the microwave frequency can be generated by the IJJ stack and mixed with the THz field down to a difference frequency of around 1.5 GHz, which was detected off-chip. These measurements show that, at least in principle, IJJ stacks can act both as THz detectors and high-frequency mixers.

In terms of emission experiments a number of early experiments were done at frequencies between a few GHz and 120 GHz, see e.g., [16, 35, 36]. Bae et al. [37] integrated oscillator and detector stacks on the same chip and found evidence for high-frequency emission up to 1 THz. Using an integrated superconducting heterodyne receiver Batov et al. [38] detected radiation at 0.5 THz from a 3 μm wide Bi-2212 mesa integrated in a bow tie antenna. The mesa consisted of about 100 IJJs. The maximum emitted power was estimated to be of the order of 0.5 pW. This emission frequency, to our knowledge, is the highest which has been detected off-chip from "small" mesa structures. Further off-chip THz emission measurements were done on stacks consisting of 700 or more IJJs with lateral sizes on the 100 μm scale. This will be addressed in detail in Section 12.4, after having introduced some theoretical concepts.

12.3 Theoretical concepts

In the previous section we did not consider in-plane degrees of freedom of IJJ stacks. For example, in sufficiently large conventional Josephson junctions fluxons (Josephson vortices) can be present and contribute to the electrodynamics of the junction. In so-called fluxon oscillators, as used in the niobium-based superconducting integrated receiver operating up to about 750 GHz [1], fluxons are created by an external magnetic field and accelerated by the applied bias current. The moving fluxons can excite standing electromagnetic waves (cavity resonances, also named Fiske modes) in the tunnel barrier. Comparatively strong and narrowband emission is obtained under these resonant conditions. The electrodynamics of long Josephson junctions is described by the sine-Gordon equation [39]. Sakai, Bodin and Pedersen extended this equation to vertically stacked Josephson junctions [40]. In the model, coupling between junctions occurs through currents flowing along the superconducting layers which are shared by adjacent junctions. This inductive coupling becomes effective when the thickness d_s of the superconducting layers inside the stack is smaller than the London penetration depth. For the case of IJJ stacks the in-plane London penetration depth $\lambda_{ab} \sim$ 150–300 nm, thus $\lambda_{ab} \gg d_s$. In the following we introduce the main ideas of the model following the notation of [41]. The geometry of N stacked long Josephson junctions is shown in Figure 12.6. $N + 1$ superconducting layers of thickness d_s are separated by insulating layers of thickness d_i. Superconducting layers are labeled from 0 to N, insulating layers from 0 to $N - 1$. An external magnetic field B (or flux Φ_ext) is oriented along y parallel to the layers. A bias current with homogeneous density j_ext is injected

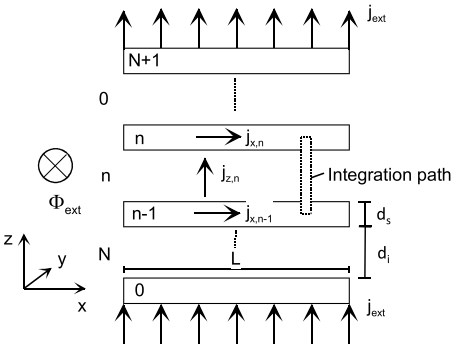

Fig. 12.6: Geometry of a stack of N long IJJs (after [41]).

into layer 0 and is extracted from layer N. The (in-plane) London penetration depth into each superconducting layer is λ_L. The length of the stack perpendicular to the magnetic field (along x) is L; all junction properties are assumed to be constant along y. The nth IJJ junction is formed by the superconducting layers $n-1$ and n and the insulating layer in between. The current density across this junction is given by

$$j_{z,n} = j_c \sin\gamma_n + \sigma_c E_{z,n} + \varepsilon\varepsilon_0 \dot{E}_{z,n} \tag{12.1}$$

The first term on the right hand side represents the Josephson current density with critical current density j_c (assumed to be the same for all layers) and the gauge invariant phase difference $\gamma_n = \varphi_n - \varphi_{n-1} - (2\pi/\Phi_0)\int_{n-1}^{n} A_z \mathrm{d}z$; n denotes the phase of the order parameter in the nth superconducting layer. A_z is the z-component of the vector potential and the dot denotes the derivative with respect to time. The second and third term on the right hand side of Equation (12.1) represent the (linearized) quasiparticle current, with c-axis conductivity σ_c and the displacement current, with dielectric constant ε. With the use of the second Josephson relation, $\dot{\gamma}_n = (2\pi/\Phi_0)E_{z,n}d_i$, also introducing normalized time $\tau = (2\pi j_c \rho_c d_i/\Phi_0)t$ and electrical field $e_z = E_z/(j_c\rho_c)$, with $\rho_c = \sigma_c^{-1}$, Equation (12.1) may be rewritten as

$$\frac{j_{z,n}}{j_c} = \sin\gamma_n + \dot{\gamma}_n + \beta_c \ddot{\gamma}_n \tag{12.2}$$

with the McCumber parameter $\beta_c = 2\pi j_c \rho_c^2 \varepsilon\varepsilon_0 d_i/\Phi_0$. The density of the supercurrent flowing along the nth superconducting layer is denoted $j_{x,n}$. Assuming the amplitude of the order parameter in the superconducting layers to be constant the phase gradient in each layer along x is given by $\partial\phi_n/\partial x = 2\pi(A_{x,n} + \mu_0\lambda_L^2 j_{x,n})/\Phi_0$. Integration of the phase gradient along the contour shown in Figure 12.6 yields

$$\frac{\mathrm{d}\gamma_n}{\mathrm{d}x} = \frac{2\pi}{\Phi_0}\left(\frac{\mathrm{d}}{\mathrm{d}x}\oint_C \boldsymbol{A}d\boldsymbol{s} + \mu_0\lambda_L^2(j_{x,n} - j_{x,n-1})\right) \tag{12.3}$$

Assuming a London magnetic field decay inside the nth superconducting layer

$$B_n(z) = \frac{B_n + B_{n+1}}{2}\frac{\cosh(z/\lambda_L)}{\cosh(d_s/2\lambda_L)} + \frac{B_{n-1} - B_n}{2}\frac{\sinh(z/\lambda_L)}{\sinh(d_s/2\lambda_L)} \tag{12.4}$$

where B_n denotes the field in the nth insulating layer one finds with the use of Maxwell's equations

$$\frac{d^2\gamma_n}{dx^2} = \frac{1}{\lambda_m^2}\frac{j_{z,n} - j_{ext}}{j_c} + \frac{1}{\lambda_k^2}\frac{2j_{z,n} - j_{z,n+1} - j_{z,n-1}}{j_c} \tag{12.5}$$

where the lengths λ_m and λ_k are given by $\lambda_m = [(\Phi_0/(2\pi j_c t_{eff})]^{0.5}$ and $\lambda_k = [\Phi_0 d_{eff}/(2\pi j_c \lambda_L^2)]^{0.5}$, with $t_{eff} = d_i + 2\lambda_L \tanh(d_s/2\lambda_L)$ and $d_{eff} = \lambda_L \sinh(d_s/2\lambda_L)$. By combining the diagonal elements on the right hand side of Equation (12.5) one may further introduce the Josephson length λ_J via $\lambda_J^{-2} = \lambda_m^{-2} + 2\lambda_k^{-2}$. If in addition in-plane quasiparticle currents, with resistivity ρ_{ab}, are taken into account, a term $(sd_s/\lambda_k^2)(\rho_c/\rho_{ab})d^2\dot{\gamma}_n/dx^2$, with $s = d_i + d_s$ should be added to the left hand side of Equation (12.5). In the limit $d_s, d_i \ll \lambda_L$, t_{eff} and d_{eff} reduce to $t_{eff} = s$ and $d_{eff} = d_s$. For the inner- and outermost junctions the terms $j_{z,n-1}$ and $j_{z,n+1}$, respectively, have to be replaced by j_{ext}. If no currents leave the stack at its left and right edges, from Equation (12.3) the boundary condition

$$\frac{d\gamma_n(x=0)}{dx} = \frac{d\gamma_n(x=L)}{dx} = \frac{2\pi}{\Phi_0} B_{ext} t_{eff} \tag{12.6}$$

can be derived. Here, self-fields due to circulating currents have been neglected.

Equations (12.5) and (12.2) form the coupled sine-Gordon equations. They can also be derived from the Lawrence–Doniach free energy for layered superconductors. This approach has been taken by several authors [42, 43]. Apart from different notations the various models also differ by the boundary conditions particularly in the z-direction. In Equations (12.5) it is demanded that the current outside the stack is given by the applied current, i.e., one considers a free standing IJJ stack. For these boundary conditions, generally, there will be fluctuating electric fields along x in the outermost electrodes. Alternatively, one may assume that the in-plane electric field is zero at the boundary [43–45], which is equivalent to treating the outermost CuO_2 layers as a ground.

For $N = 1$ Equations (12.5) and (12.2) reduce to the standard sine-Gordon equation, containing λ_J as the only relevant length scale. For stacked junctions λ_k appears as an additional scale. For a critical current density of 200 A/cm^2, a typical value for IJJs, and $\lambda_{ab} = 0.26\,\mu m$ one finds $\lambda_m = 295\,\mu m$, $\lambda_k = 0.76\,\mu m$ and $\lambda_J = 1.07\,\mu m$. For an IJJ stack with lateral dimension below 1 μm the coupling between adjacent IJJs is small and the stack forms in essence a series array of independent junctions. For larger lateral sizes of the stack the scale λ_k matters as soon as $j_{z,n}$ and $j_{z,n\pm1}$ are different, in other words, as soon as there is a gradient along z in the in-plane currents. In the absence of such gradients even stacks with a lateral size of 300 μm could behave as an array of independent short junctions. However, in general there will be the formation of circulating currents and the junctions in the stack become coupled.

Let us give us an example for the simulated collective fluxon dynamics in a 10 μm long 20-junction stack. Figure 12.7 displays the IVC for zero applied magnetic field.

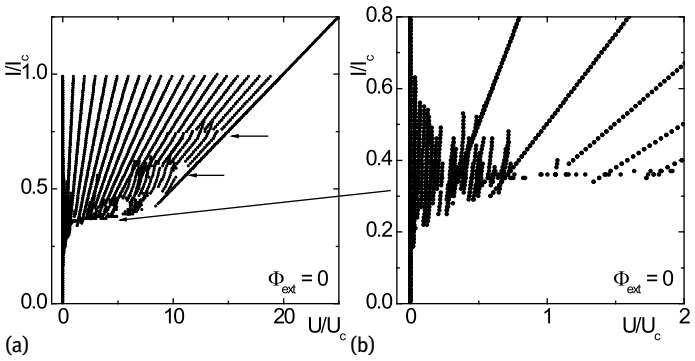

Fig. 12.7: Calculated IVC of a 20-junction stack in zero magnetic field showing 20 linear resistive branches and a variety of resonant structures and zero field steps, indicated by arrows (a). The low-voltage region is enlarged in (b) (after [41]).

Multiple branching still occurs, consistent with the experimental observation. There are also fine structures which in the simulation are due to different dynamic fluxon configurations. Figure 12.8 shows two snapshots of the Josephson currents in the stack for $I = 0.55\, I_c$. There are fluxons (antifluxons) in the stack, the center of which is marked by closed (open) circles. The fluxons and antifluxons are aligned in vertical rows moving in opposite direction. At $t = 0$ most vortices are located in the odd-labeled junctions whereas, after reflection at the edges fluxons move in the even-labeled junctions. A similar switching by one junction occurs when the vortex/antivortex columns collide in the middle of the stack. The second snapshot is in fact taken after a half period of this periodic dynamics. Further, all junctions are in a nonzero-voltage state, and the fluxon motion in the inner junctions 4 to 17 is synchronous, as can be seen from the fact that the dc voltage across these junctions is identical. At the vortex collision points, which for the locked IJJs always occurs at the same x coordinate, the amplitude of the electric fields in the barrier layers of the various IJJs is at its maximum, in other words the antinode of a standing wave develops at these locations. Thus, the electric field, on top of an offset, indeed exhibits a well-developed standing wave pattern with three half-waves along x and one half-wave along z (the corresponding snapshots are not shown explicitly here). It further turns out that some of the IJJs can be in the zero-voltage state, never containing fluxons, without significantly disturbing the pattern shown in Figure 12.8. This explains why the multiple branching can be obtained for the IVCs of IJJ stacks despite complex internal dynamics.

The state described above is an example of a fluxon state involving the excitation of a collective resonance using the whole stack as a cavity. There is in fact a variety of different collective cavity modes [46, 47]. For the boundary conditions used above the electric field for these modes in 3D for a rectangular N junction stack of length L and

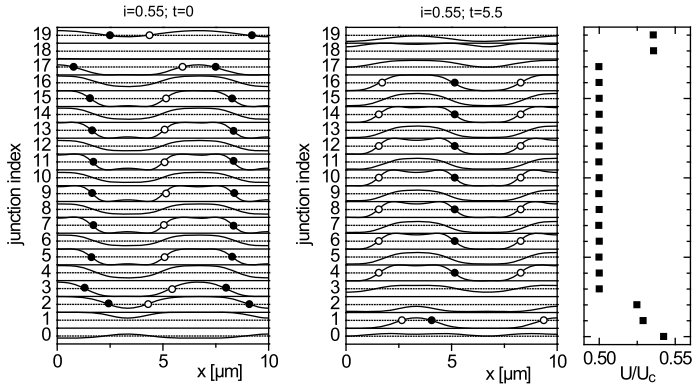

Fig. 12.8: Two snapshots of supercurrent distribution for $i = I/I_c = 0.55$, cf. Figure 12.7, together with the dc voltage across each junction (right). Fluxon centers are marked by closed circles, centers of antifluxons by open circles. Fluxon motion is towards the left edge, antifluxons move towards the right edge (after [41]).

width W have a component

$$E_{z,n}(x,y) = E_0 \cos(\omega_{qk_xk_y} t) \sin\left(\frac{\pi nq}{N+1}\right) \cos\left(\frac{\pi k_x x}{L}\right) \cos\left(\frac{\pi k_y y}{W}\right) \tag{12.7}$$

with some amplitude E_0 and integers k_x and k_y counting the number of half-waves along x and y, respectively. The integer q runs from 1 to N. The frequencies $\omega_{qk_xk_y}$ are given by

$$\omega^2_{qk_xk_y} = \omega^2_{\mathrm{pl}} \sqrt{1-(I/I_c)^2} + c_q^2 \left[\left(\frac{\pi k_x}{L}\right)^2 + \left(\frac{\pi k_y}{W}\right)^2\right] \tag{12.8}$$

where $\omega_{\mathrm{pl}} = (2\pi t_{\mathrm{eff}} j_c/\Phi_0 \varepsilon\varepsilon_0)^{0.5}$ is the Josephson plasma frequency. The velocities c_q are given by

$$c_q = \frac{\omega_{\mathrm{pl}} \lambda_J}{\sqrt{1-2\bar{s}\cos[\pi q/(N+1)]}} \tag{12.9}$$

$\bar{s} = (\lambda_J/\lambda_k)^2$ denotes the coupling parameter [40]. For $q = 1$ all junctions oscillate in-phase, which is apparently the most interesting situation for THz emission. For large values of N the mode velocity c_1 can be very high, reaching values of the order of $c/\sqrt{\varepsilon}$, with the vacuum speed of light c. We briefly note here that the expression for c_q changes when using different boundary conditions along z. For example, for a mesa structure one may consider the base crystal as a ground. Then, on the right hand sides of Equations (12.7) and (12.9) the factor $(N+1)$ should be replaced by $(2N+1)$ and q by $2q-1$. If in-plane electric fields vanish on both outermost faces of the stack in Equation (12.7) the sine function should be replaced by a cosine and $(N+1)$ by N. Here, the value $q = 0$ becomes an allowed solution.

The excitation of the in-phase cavity mode by Josephson vortices has been studied in detail by Koshelev [44, 48] and by Lin and Hu [45, 49]. It turned out that the

Josephson phases along the different junctions can contain a term of π phase kinks and antikinks arranged periodically in the z-direction, with integer m. These π phase kinks effectively excite the various cavity modes. These can also be efficiently excited by fluxon lattices created by applying high magnetic fields oriented parallel to the layers [46]. This type of excitation is analogous to the mechanism used in the fluxon oscillator of the superconducting integrated receiver.

In experiments using small-sized IJJ stacks with $N < 100$, there was no clear evidence for resonant modes in zero applied field. Collective Fiske modes were observed in strong magnetic fields [37, 50–52] and perhaps also under microwave radiation [53, 54], with mode velocities that were consistent with theoretical considerations. However, dominantly the modes with large values of q – i.e., modes where the IJJs in the stack oscillate dominantly out-of-phase and produce very little radiation – were excited. The situation is opposite for very large stacks consisting of hundreds of IJJs. Here, the in-phase modes turn out to be the most stable. The corresponding experiments will be addressed in Section 12.4.

We conclude this section by noting that the inductive coupling is not the only possible interaction between adjacent IJJs. The thickness of the superconducting layers is in fact comparable or even smaller than the Debye screening length which can be estimated to be of the order of 2–3 Å for Bi-2212. One of the effects that can occur is that there are local charges in the superconducting layers felt by adjacent junctions. As a consequence the second Josephson relation is modified and the time evolution of the phase of the nth junction depends not only on the electric field across this junction but also on the electric field across its neighbors. This type of coupling has been pointed out by Koyama and Tachiki [55] and has been studied later on in a number of publications [56–60]. Second, there can be an imbalance between electron-like and hole-like quasiparticle excitations again affecting the system dynamics. A detailed description of the charging effects including also effects of branch imbalance has been given by several authors [61–63]. The charge coupling affects the dynamics of the IJJ stack near the lower end of a given branch of the IVC (i.e., near the return current). The impact of charge coupling on coherent THz emission, as obtained for the large IJJ stacks, is not fully clarified yet but seems to be less important than inductive coupling.

12.4 Coherent THz radiation from large intrinsic Josephson junction stacks

In 2007 Ozyuzer et al. reported THz emission from IJJ stacks where the junctions in the stack oscillated in-phase [12]. The stacks were patterned as mesa structures on top of Bi-2212 single crystals. With a length of more than 300 µm, widths of several 10 µm and a thickness of about 1 µm, corresponding to ~700 IJJs these stacks were much larger than the stacks studied previously. Experiments were performed in zero

magnetic field. This result was unexpected since such large stacks were expected to heat up to temperatures well above T_c. Figure 12.9 shows (a,b) the geometry and (c,d) selected results. The IVC (Figure 12.9c, right scale; only the return branch with all IJJs in the resistive state is shown), measured at a bath temperature $T_{bath} = 25$ K indeed exhibits the strong back-bending which is due to overheating. Some numbers for the average stack temperature, as estimated from the temperature dependence of the out-of-plane resistivity, are indicated. For a current of 25 mA the estimated temperature is 85 K, at an input power of about 25 mW. This overheating of about 60 K is strong but in fact much less than the numbers found for small mesas (sometimes exceeding 20 K per mW). Polarized THz emission was detected in the lower current range where Joule heating is modest. The maximum *detected* radiation power (Figure 12.9c, left scale) was about 10 nW which, extrapolated to 4π, amounted to about 0.5 μW, at frequencies up to 0.85 THz and for bath temperatures up to 50 K. Further, it was found that the emission frequency scaled with the width of the stack, cf. Figure 12.9d, indicating that a cavity resonance oscillating along the width is important for synchronization. The cavity resonance is indicated schematically in Figure 12.9a.

Reference [12] triggered a large mount of theoretical and experimental investigations; more than 100 publications have appeared by now. Below we can only mention a few results.

Figure 12.10 shows results of an investigation of large IJJ mesas using low-temperature scanning laser microscopy (LTSLM) [64]. In LTSLM a blanked laser beam is scanned across the sample surface while the sample is biased at some current I. At the position (x_L, y_L) of the beam the temperature of the sample locally rises by a few K and, as a result, temperature-dependent quantities like the junction resistance or the critical current density change. These changes lead to a variation $\Delta V(x_L, y_L)$ of the voltage across the stack which serves as the contrast for an LTSLM image. For IJJ stacks LTSLM revealed two different features. In LTSLM image B of Figure 12.10 there are two stripelike features separated by a low-contrast region. With increasing input power the left stripe moves towards the left edge of the stack. This feature has been identified at the edge of a "hot spot", separating a region which is heated to temperatures well above T_c and a region which is still superconducting. The appearance of a hot spot has been confirmed by thermoluminescence measurements [65–67]. According to these measurements the maximum temperature in the hot spot can exceed 150 K. In the "cold" part of the stack in the LTSLM data of Figure 12.10 additional stripes appear, having a lower contrast ΔV than the signal associated with the hot-spot edges. These signals can in fact be attributed to standing electromagnetic waves, the maxima (in $|\Delta V|$) marking the antinodes of the cavity resonances [64, 68, 69]. The importance of geometric resonances has been stressed in several papers, see. e.g., [70, 71].

Further, by varying the bath temperature T_{bath} the voltage across the IJJ stacks can be varied over a significant range, allowing us to test whether or not the observed THz emission arises from the Josephson effect. So far all experiments indeed show that the Josephson frequency-voltage relation is fulfilled.

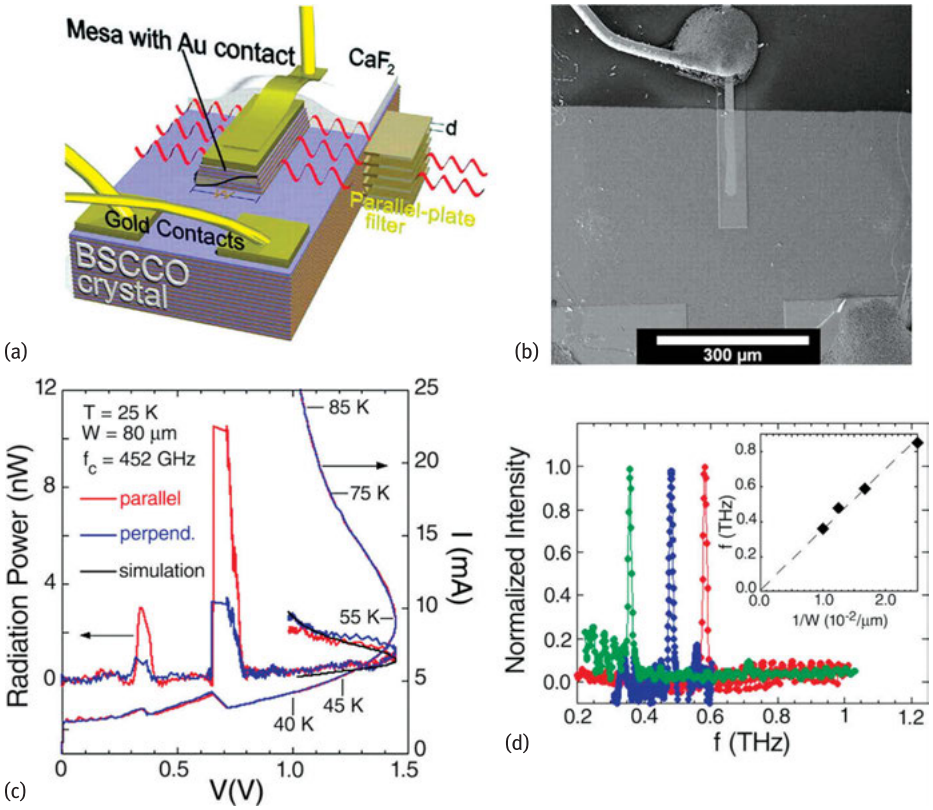

Fig. 12.9: THz emission from large Bi-2212 mesas. (a) Schematic of mesa. (b) SEM image. (c) Radiation power (left) and IVC (right). (d) Fourier spectra of emitted radiation for mesas of different width. Inset shows dependence of radiation frequency on reciprocal width. In (c) "parallel" and "perpendicular" refer to the orientation of the parallel-plate filter, having a cutoff-frequency $f_c = 452$ GHz. From [12].

Shortly after the discovery of in-phase THz radiation also the angle dependence of the emitted radiation power has been measured [72]. It turned out that for rectangular mesas the emission power is relatively large in the c-direction and has its maximum at a tilt of about 30° from the c-axis. The emission power is very low in the direction parallel to the base crystal. This indicates that the IJJ stack cannot simply be considered as a source of electric dipole radiation. Magnetic components also play an important role; in addition the base crystal seems not to favor THz emission.

There has been some debate whether the hot spot just coexists with the superconducting areas [66] or has a direct effect on THz radiation. Evidence for the latter scenario comes from high-resolution measurements of the linewidth Δf_e of THz radiation [73]. For the investigated mesas, in the absence of a hot spot, Δf_e was 0.5 GHz or higher, i.e., one observes a ratio $f_e/\Delta f_e$ typically well below 1000. In the presence of

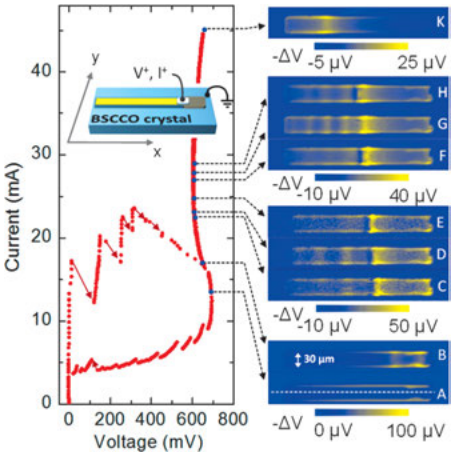

Fig. 12.10: IVC and LTSLM data of a 30×330 µm^2 large Bi-2212 mesa at $T_{bath} = 50$ K. Red solid arrows in the IVC denote switching processes, black arrows indicate bias points where LTSLM images A–K have been taken. After [64].

a hot spot, Δf_e was as low as 23 MHz at $f_e = 0.6$ THz, i.e., $f_e/\Delta f_e \approx 3 \cdot 10^4$. Further, Δf_e was found to *decrease* with increasing bath temperature. By contrast, if phase synchronization of the IJJs in the mesas were only mediated by cavity resonances one would expect $f_e/\Delta f_e$ to be proportional to the quality factor of the cavity mode which should decrease with increasing temperature (either bath temperature or actual temperature in the stack).

The experimental observations introduced so far – the interaction of Josephson currents and cavity modes, the appearance of a hot spot, the unusual dependence of the linewidth of radiation on temperature in the presence of the hot spot and the angle dependence of radiation – have been addressed in numerous theoretical works. In parallel there were significant experimental efforts to improve the performance of the IJJ emitters in terms of emission power, maximum emission frequency, tunability and thermal handling. Let us start with some theoretical concepts and then turn to experimental efforts.

A number of works, based on inductively coupled sine-Gordon equations, addressed the mechanisms to excite collective cavity resonances in the stack [44, 45, 48, 49, 74–76]. To excite such modes it is favorable to have some initial modulation of the Josephson current and the ac electric field that are commensurate with the cavity mode to be excited. It was found that vertically stacked $\pm\pi$ kinks in the Josephson phase differences can form, couple effectively to cavity modes and synchronize ac Josephson oscillations. Three examples for π-phase kink states are shown in Figure 12.11. THz emission properties were also calculated in simulations based on sine-Gordon type models and the radiation patterns observed experimentally have been partially reproduced [74, 75, 77, 78]. It was pointed out that in-plane dissipation, often neglected in simulations, can play an important role in achieving in-phase synchronization [79].

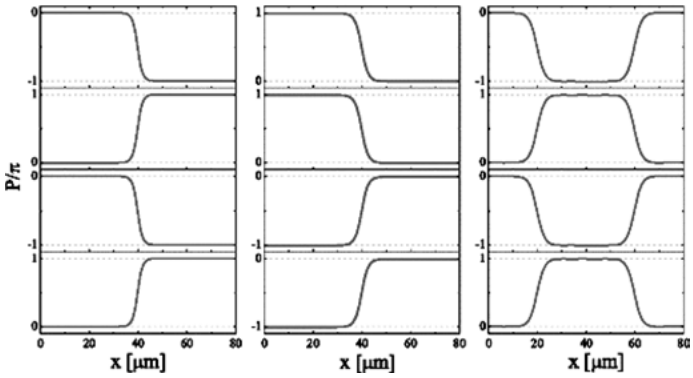

Fig. 12.11: Typical π-phase kink states (static contribution to the Josephson phase differences $\gamma(x)$) forming in IJJ stacks (four adjacent IJJs are shown). From [45].

A second line of theoretical investigations addressed hot spot formation on the basis of heat diffusion equations, taking into account only quasiparticle currents [80–82]. Very good agreement with experimental data was achieved, reproducing the typical back-bending of the IVCs and hot spot formation, respectively. The latter occurs in the back-bending regime and is due to the specific temperature dependence of the Bi-2212 *c*-axis resistivity. When, due to some fluctuation, the temperature in a part of the stack increases, the local *c*-axis resistivity decreases, leading to an increase in the applied current density and also the local heat production. The cycle continues until equilibrium is reached. The effect is in fact not specific to IJJ stacks but has been observed for many conducting systems [83]. A very early work on this phenomenon has been presented in the context of semiconductors [84].

The next step for theory was to combine electromagnetic and thermal properties of the IJJ stacks. In [80] the hot spot was modeled as a 2D array of resistors and capacitors which was coupled to a serial array of pointlike Josephson junctions representing the cold part of the stack. It was observed that the currents through the hot spot area can phase-lock the Josephson junction array. In [85] THz radiation from IJJ stacks was modeled in 3D introducing the hot spot as a predefined region of reduced Josephson critical current density. A three-step approach to fully combine Josephson dynamics and thermal physics was given in Refs. [86–88]. In a first step the mesa was replaced by two parallel columns of electrically coupled pointlike Josephson junctions which were also coupled to a thermal bath. The $N = 700$ junctions were grouped to M segments, each containing $G = N/M$ IJJs assumed to be identical. The parameters of the model (Josephson critical current, resistance) depend on the local temperature which in turn is calculated by the heat diffusion equation containing the Joule heat production as the input from the electrical circuit. Within this model it was possible to investigate IVCs, reproduce the formation of hot spots (one of the chains of junctions at a temperature above T_c) and also the linewidth of THz radiation as a function of T_{bath}.

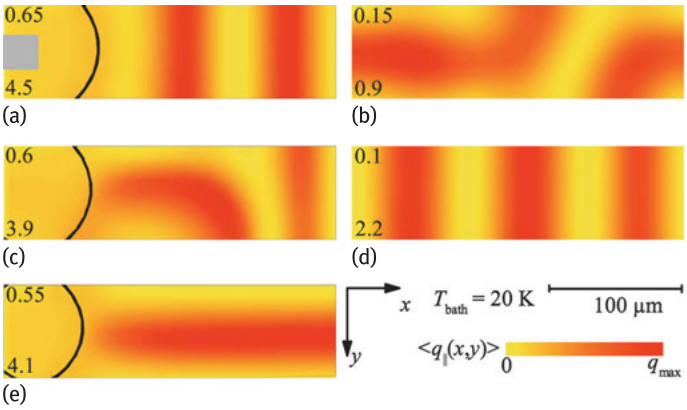

Fig. 12.12: Normalized power density $\langle q_{\|}(x, y)\rangle$ (in units of 400 W/cm^3) dissipated by in-plane currents, averaged over time and z, for five values of normalized bias current I/I_{c0} (upper left numbers); values for q_{max} at bottom left. The gray square in (a) indicates the position of the bond wire attached to the mesa and included in the thermal part of the equations. Regions enclosed by the black line are at $T \geq T_c$. From [88].

Currents through the hot areas provided phase-lock between the junctions that were in the superconducting state. The experimentally observed decrease of Δf_e with increasing bath temperature was reproduced and attributed to a competition between the ability of the system to phase-lock (increasing with increasing temperature) and the destructive effects of thermal fluctuations and the relative spread in junction parameters (also growing with increasing bath temperature). In a second and third step the approach of [86] was extended to 1D-coupled sine-Gordon equations [87] and finally to full 3D simulations [88]. These simulations quantitatively reproduced the formation of hot spots and the appearance of cavity modes. Figure 12.12 shows, for $T_{bath} = 20$ K, averaged distributions of the power density $\langle q_{\|}(x, y)\rangle$ dissipated by in-plane currents for five values of $I/I_{c0} = 0.65$ (a) to 0.1 (e). Averaging is over time and the c-direction in the mesa. This type of plot is used to visualize resonance patterns, with nodes (antinodes) appearing at the minima (maxima) of $\langle q_{\|}(x, y)\rangle$. The left (right) graphs are at high (low) bias where a hot spot is present (absent). In (a) and (e) the modulations along x are due to a cavity mode oscillating along x (a $(0, n)$ mode, with $n = 2$ and 3, respectively). In (c) a cavity mode oscillating along y is excited (a $(1, 0)$ mode). The spatial variations in (b) and (d) have a more complicated mixed structure. The $(1, 0)$ mode is the one proposed in [12] for phase synchronization. The 3D simulations in fact revealed that, by applying a small magnetic field parallel to the long side of the stack, this mode can be stabilized over a wide range of bias currents and bath temperatures. The prediction was also tested experimentally, resulting in an increase of the THz emission power of up to a factor of 2.7 [88].

We return to experimental investigations. Besides mesa structures, a variety of different structures have been realized, including all-superconducting Z-type stacks [89]

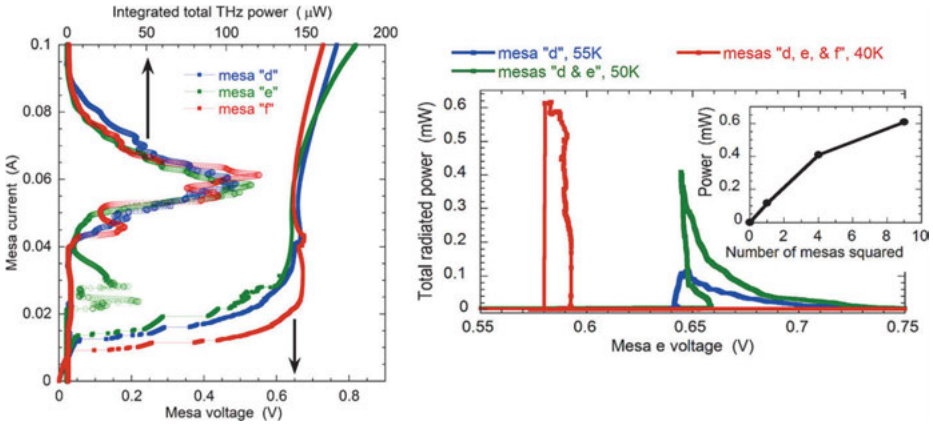

Fig. 12.13: IVCs and THz emission characteristics of a parallel array of mesas patterned on the same base crystal. Left: Characteristics of three of the mesas when biased separately at $T_{bath} = 55$ K. Right: Total radiation power versus bias voltage across mesa (e) for simultaneous bias of some mesas. From [99].

and stand-alone stacks embedded between Au layers [71, 90–93]. The emission power obtained from the stand-alone stacks is often much higher than the one from mesas, reaching values of up to 80 μW [90, 93–95]. Cooling has been improved further by sandwiching the stand-alone stacks between substrates with high thermal conductivity. In first attempts maximum emission frequencies near 1.05 THz were obtained [92, 96]. Recently this value was improved to more than 1.6 THz for rectangular stand-alone stacks [93, 97] and to 2.4 THz for disk-shaped stand-alone stacks [98].

The stacks investigated in [93, 97, 98] partially consisted of more than 2000 IJJs. It seems unlikely that this number can be increased significantly, say to more than 10 000 IJJs. A way to further increase the output power is to use arrays of stacks. Benseman et al. [99] investigated a set of six 400×60 μm^2 large 500-junction mesas fabricated on the same base crystal. Adjacent mesas were separated by 60 μm. The left graph of Figure 12.13 shows IVCs and the THz emission power for three individual mesas. The maximum power was of the order of 120 μW. When biasing some of the mesas simultaneously, after optimizing the response, an output power of about 0.6 mW was achieved at an emission frequency of 0.51 THz. This, up to now, is the record value and has not yet been reproduced, underlining the difficulty to actually achieve phase synchronization between different mesas.

Both for single stacks and for arrays of stacks tunability is an issue. By changing T_{bath} and the bias current the emission frequency can be varied over a wide range. However, the emission power P_e may not always be at its optimum. For instance, in the high-bias regime the position of the hot spot strongly affects P_e. However, the problem can be overcome by using stand-alone stacks contacted by three electrodes [100]. One terminal is used as a collective ground while the other two, contacting the stack from

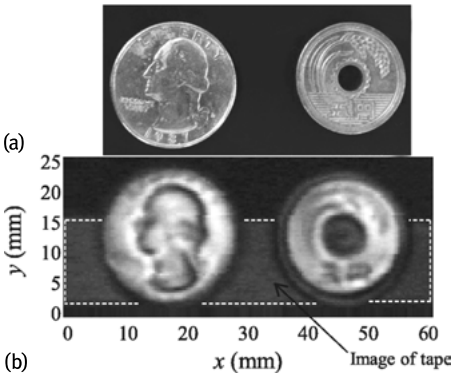

Fig. 12.14: Reflection imaging at 0.44 THz of different coins using a Bi-2212 IJJ mesa as oscillator. (a) Photographs of the US quarter coin and the Japanese 5-yen coin. (b) Reflection images of both coins. From [103].

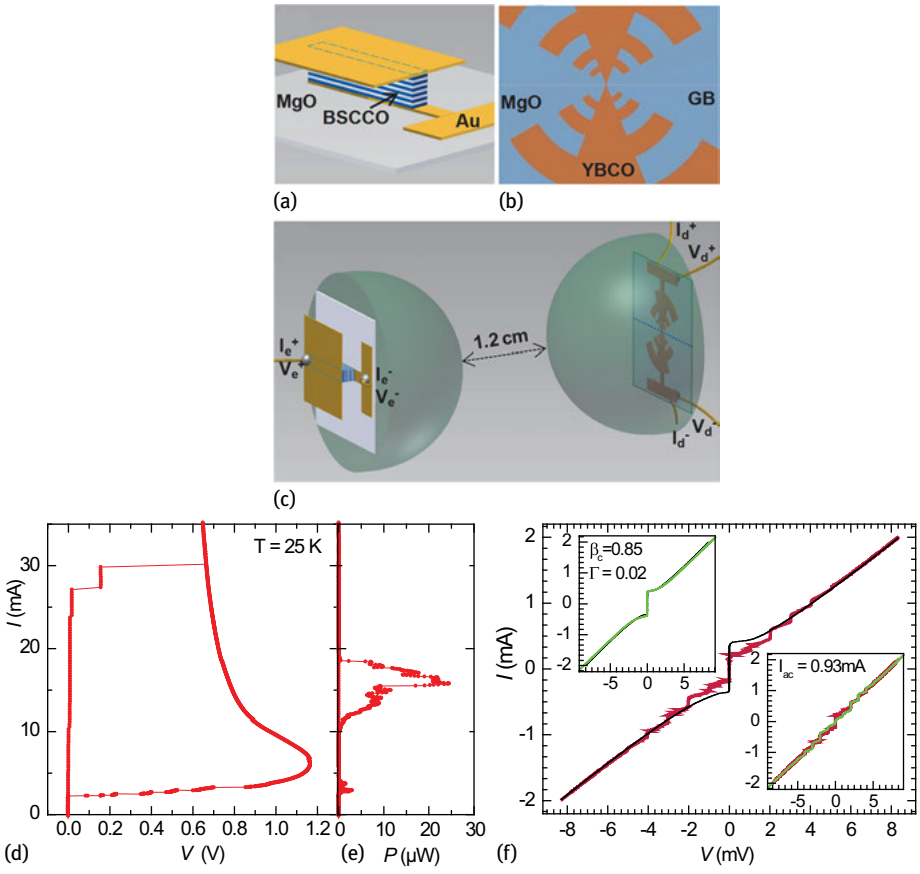

Fig. 12.15: Setup combining a Bi-2212 intrinsic junction stack emitter and a YBCO grain boundary junction detector. Upper graphs show the schematics of (a) the Bi-2212 emitter, (b) the detector based on a $YBa_2Cu_3O_7$ grain boundary (GB) Josephson junction and (c) the detector and emitter mounted on hyper-hemispheric Si lenses. The lower graphs show the IVC (a) and the THz emission signal (b) of the Bi-2212 emitter, and (c) IVCs of the detector junction with and without irradiation from the emitter. Insets compare both IVCs of the detector with simulations. From [90].

its right and left side, allow one to vary the current injection profile. With this method both the hot-spot position and P_e can be varied reproducibly. The hot spot can also be manipulated by using a laser beam [101, 102]. However, this procedure may be too sophisticated at least for some applications.

Using Bi-2212 stacks some potential applications have been demonstrated. Tsujimoto et al. [104] used a $400 \times 62 \times 1.9\,\mu m^3$ large mesa structure as an oscillator to perform absorption imaging at frequencies around 0.5–0.6 THz of Japanese coins and a razor blade placed inside paper envelopes. Kashiwagi et al. extended this technique to reflection imaging [103] and computed tomography imaging [105]. Two reflection images of coins are shown in Figure 12.14. An et al. [90] demonstrated an all-high T_c emitter-receiver setup using a Bi-2212 stack as emitter and a $YBa_2Cu_3O_7$ grain boundary junction integrated into a logarithmic-periodic antenna as the receiver. The setup and some data are shown in Figure 12.15. Under 0.52 THz irradiation generated by the emitter the detector junction exhibited clear Shapiro steps, allowing, e.g., one to analyze the emission frequency and power received from the Bi-2212 emitter. Further, Bi-2212 stacks have been operated in a miniaturized and battery-driven setup operating in liquid nitrogen [106].

These examples may show that in the past years significant progress has been made in the development of Bi-2212-based THz oscillators. However, one should emphasize that still many tasks need to be solved. The numbers given above for emission power, emission frequency, linewidth of radiation etc., are for the best samples and nobody has succeeded yet in combining them in one and the same device. Also, improving reproducibility is an issue. These are tasks to be solved in the near future.

Acknowledgment: We gratefully acknowledge financial support by the National Natural Science Foundation of China (Grant Nos. 11234006 and 61501220), the Priority Academic Program Development of Jiangsu Higher Education Institutions, Jiangsu Provincial Natural Science Fund (BK20150561), the Deutsche Forschungsgemeinschaft (Project KL930/13-1), JSPS KAKENHI Grant Number 25289108 and the EU-FP6-COST Action MP1201.

Bibliography

[1] Koshelets VP, Shitov SV. Integrated superconducting receivers. Supercond. Sci. Technol. 13:R53, 2000.

[2] Darula M, Doderer T, Beuven S. Millimetre and sub-mm wavelength radiation sources based on discrete Josephson junction arrays. Supercond. Sci. Technol. 12:R1, 1999.

[3] Barbara P, Cawthorne AB, Shitov SV, Lobb CJ. Stimulated emission and amplification in Josephson junction arrays. Phys. Rev. Lett. 82:1963, 1999.

[4] Song F, Müller F, Behr R, Klushin M. Coherent emission from large arrays of discrete Josephson junctions. Appl. Phys. Lett. 95:172501, 2009.

[5] Galin MA, Klushin AM, Kurin VV, Seliverstov SV, Finke MI, Goltsman GN, Müller F, Scheller T, Semenov AD. Towards local oscillators based on arrays of niobium Josephson junctions. Supercond. Sci. Technol. 28:055002, 2015.
[6] Kleiner R, Steinmeyer F, Kunkel G, Müller P. Intrinsic Josephson effects in $Bi_2Sr_2CaCu_2O_8$ single crystals. Phys. Rev. Lett. 68:2394, 1992.
[7] Ferguson B, Zhang XC. Materials for terahertz science and technology. Nat. Mat. 1:26, 2002.
[8] Tonouchi M. Cutting-edge terahertz technology. Nat. Photon. 1:97, 2007.
[9] Pedersen NF, Ustinov AV. Fluxons in Josephson transmission lines: new developments. Supercond. Sci. Technol. 8:389, 1995.
[10] Yurgens AA. Intrinsic Josephson junctions: recent developments. Supercond. Sci. Technol. 13:R 85, 2000.
[11] Hu X, Lin SZ. Phase dynamics in a stack of inductively coupled intrinsic Josephson junctions and terahertz electromagnetic radiation. Supercond. Sci. Technol. 23:053001, 2010.
[12] Ozyuzer L, Koshelev AE, Kurter C, Gopalsami N, Li Q, Tachiki M, Kadowaki K, Yamamoto T, Minami H, Yamaguchi H, Tachiki T, Gray KE, Kwok W-K, Welp U. Emission of coherent THz radiation from superconductors. Science 318:1291, 2007.
[13] Savel'ev S, Yampol'skii VA, Rakhmanov AL, Nori F. Terahertz Josephson plasma waves in layered superconductors: spectrum, generation, nonlinear and quantum phenomena. Rep. Prog. Phys. 73:026501, 2010.
[14] Welp U, Kadowaki K, Kleiner R. Superconducting emitters of THz radiation. Nat. Photon. 7:702, 2013.
[15] Odagawa A, Sakai M, Adachi H, Setsune K, Helm C, Kleiner R. Observation of microwave induced steps for a single intrinsic tunnel junction. Advances in Superconductivity IX, Proceedings of the 11th International Symposium on Superconductivity (ISS '98), November 16–19, 1998, Fukuoka, Springer, Japan, 1147, 1999.
[16] Kleiner R, Müller P. Intrinsic Josephson effects in high-T_c superconductors. Phys. Rev. B 49:1327, 1994.
[17] Odagawa A, Sakai M, Adachi H, Setsune K. I-V characteristic of a single intrinsic tunnel junction on Bi2223 thin film. IEEE Trans. Appl. Supercond. 9:3012, 1999.
[18] Yurgens A, Winkler D, Claeson T, Murayaha T, Ando Y. Effect of pressure on interlayer coupling and superconducting transition temperature of Bi-2201 and Bi-2212. Int. J. Mod. Phys. B 13:3744, 1999.
[19] Ueda S, Yamaguchi T, Kubo Y, Tsuda S, Shimoyama J, Kishio K, Takano Y. Switching current distributions and subgap structures of underdoped (Hg,Re)$Ba_2Ca_2Cu_3O_{8+\delta}$ intrinsic Josephson junctions. J. Appl. Phys. 106:074516, 2009.
[20] Chana OS, Kuzhakhmetov AR, Warburton PA, Hyland DMC, Dew-Hughes D, Grovenor CRM, Kinsey RJ, Burnell G, Booij WE, Blamire MG, Kleiner R, Müller P. Alternating current Josephson effect in intrinsic Josephson bridges in $Tl_2Ba_2CaCu_2O_8$ thin films. Appl. Phys. Lett. 76:3603, 2000.
[21] Kim S-J, Latyshev YuI, Yamashita T. 3D intrinsic Josephson junctions using *c*-axis thin films and single crystals. Supercond. Sci. Technol. 12:729, 1999.
[22] Kawakami T, Suzuki M. Direct observation of intrinsic Josephson junction characteristics in electron-doped $Sm_{2-x}Ce_xCuO_{4-\delta}$. Supercond. Sci. Technol. 26:093002, 2013.
[23] Nachtrab T, Koelle D, Kleiner R, Bernhard C, Lin CT. Intrinsic Josephson effects in the magnetic superconductor $RuSr_2GdCu_2O_8$. Phys. Rev. Lett. 92:117001, 2004.
[24] Schlenga K, Biberacher W, Hechtfischer G, Kleiner R, Schey B, Waldmann O, Walkenhorst W, Müller P. Intrinsic Josephson effects in various layered superconductors. Physica C, 235–240:273, 1994.

[25] Moll PJW, Zhu X, Cheng P, Wen H-H, Batlogg B. Intrinsic Josephson junctions in the iron-based multi-band superconductor $(V_2Sr_4O_6)Fe_2As_2$. Nature Physics 10:644, 2014.
[26] Schlenga K, Hechtfischer G, Kleiner R, Walkenhorst W, Müller P, Johnson HL, Veith M, Brodkorb W, Steinbeiss E. Subgap structures in intrinsic Josephson junctions of $Tl_2Ba_2Ca_2Cu_3O_{10}$ and $Bi_2Sr_2CaCu_2O_{8+\delta}$. Phys. Rev. Lett. 76:4943, 1996.
[27] Wang HB, Wu PH, Chen J, Maeda K, Yamashita T. 3-dimensional arrays of BiSrCaCuO-2212 intrinsic Josephson junctions and the zero-crossing Shapiro steps at 760 GHz. Appl. Phys. Lett. 80:1604, 2002.
[28] Wang HB, You LX, Chen J, Wu PH, Yamashita T. Observation of Shapiro steps and spectroscopic applications of stacked intrinsic Josephson junctions up to the terahertz region. Supercond. Sci. Technol. 15:90, 2002.
[29] Bae M-H, Lee H-J, Kim J, Kim K-T. Microwave distribution in stacked $Bi_2Sr_2CaCu_2O_{8+x}$ intrinsic Josephson junctions in a transmission-line geometry. Appl. Phys. Lett. 83:2187, 2003.
[30] Helm Ch, Preis Ch, Forsthofer F, Keller J, Schlenga K, Kleiner R, Müller P. Coupling between phonons and intrinsic Josephson oscillations in cuprate superconductors. Phys. Rev. Lett. 79:737, 1997.
[31] Tsvetkov AA, Dulić D, van der Marel D, Damascelli A, Kaljushnaia GA, Gorina JI, Senturina NN, Kolesnikov NN, Ren ZF, Wang JH, Menovsky AA, Palstra TTM. Systematics of *c*-axis phonons in the thallium- and bismuth-based cuprate superconductors. Phys. Rev. B 60:13196, 1999.
[32] Wang HB, Wu PH, Yamashita T. Terahertz responses of intrinsic Josephson junctions in high T_c supercondctors. Phys. Rev. Lett. 87:107002, 2001.
[33] Rother S, Kleiner R, Müller P, Darula M, Kasai Y, Nakajima K. Far infrared response of intrinsic Josephson junctions. Physica C 341:1565, 2000.
[34] Rother S, Koval Y, Müller P, Kleiner R, Kasai Y, Nakajima K, Darula M. FIR response of intrinsic Josephson junctions. IEEE Trans. Appl Supercond. 11:1191, 2001.
[35] Walkenhorst W, Hechtfischer G, Schlötzer S, Kleiner R, Müller P. Probing the collective Josephson plasma resonance in $Bi_2Sr_2CaCu_2O_{8+y}$ by *W*-band-mixing experiments. Phys. Rev. B 56:8396, 1997.
[36] Lee K, Wang W, Iguchi I, Tachiki M, Hirata K, Mochiku T. Josephson plasma emission from $Bi_2Sr_2CaCu_2O_y$ intrinsic junctions due to quasiparticle injection. Phys. Rev. B 61:3616, 2000.
[37] Bae MH, Lee H-J, Choi J-H. Josephson-vortex-flow terahertz emission in layered high-T_c superconducting single crystals. Phys. Rev. Lett. 98:027002, 2007.
[38] Batov I, Jin X, Shitov S, Koval Y, Müller P, Ustinov A. Detection of 0.5 THz radiation from intrinsic $Bi_2Sr_2CaCu_2O_8$ Josephson junctions. Appl. Phys. Lett. 88:262506, 2006.
[39] Barone A, Esposito F, Magee CJ, Scott AC. Theory and applications of the sine-Gordon equation. Rivista del Nuovo Cimento 1:227, 1971.
[40] Sakai S, Bodin P, Pedersen NF. Fluxons in thin-film superconductor-insulator superlattices. J. Appl. Phys. 73:2411, 1993.
[41] Kleiner R, Gaber T, Hechtfischer G. Stacked long Josephson junctions in zero magnetic field: A numerical study of coupled one-dimensional sine-Gordon equations. Phys. Rev. B 62:4086, 2000.
[42] Bulaevskii LN, Zamora M, Baeriswyl D, Beck H, Clem JR. Time-dependent equations for phase differences and a collective mode in Josephson-coupled layered superconductors. Phys. Rev. B 50:12831, 1994.
[43] Koshelev AE. Role of in-plane dissipation in dynamics of a Josephson vortex lattice in high-temperature superconductors. Phys. Rev. B 62:R3616, 2000.
[44] Koshelev AE. Alternating dynamic state self-generated by internal resonance in stacks of intrinsic Josephson junctions. Phys. Rev. B 79:174509, 2008.

[45] Lin SZ, Hu X. Possible dynamic states in inductively coupled intrinsic Josephson junctions of layered high-T_c superconductors. Phys. Rev. Lett. 100:247006, 2008.
[46] Kleiner R. Two-dimensional resonant modes in stacked Josephson junctions. Phys. Rev. B 50:6919, 1994.
[47] Sakai S, Ustinov AV, Kohlstedt H, Petraglia A, Pedersen NF. Theory and experiment on electromagnetic-wave-propagation velocities in stacked superconducting tunnel structures. Phys. Rev. B 50:12905, 1994.
[48] Koshelev AE. Stability of dynamic coherent states in intrinsic Josephson-junction stacks near internal cavity resonance. Phys. Rev. B 82:174512, 2010.
[49] Hu X, Lin SZ. Three-dimensional phase-kink state in a thick stack of Josephson junctions and terahertz radiation. Phys. Rev. B 78:134510, 2008.
[50] Krasnov VM, Mros N, Yurgens A, Winkler D. Fiske steps in intrinsic $Bi_2Sr_2CaCu_2O_{8+x}$ stacked Josephson junctions. Phys. Rev. B 59:8463, 1999.
[51] Wang HB, Urayama S, Kim SM, Arisawa S, Hatano T, Zhu BY. Terahertz oscillation in submicron sized intrinsic Josephson junctions. Appl. Phys. Lett. 89:252506, 2006.
[52] Katterwe SO, Rydh A, Motzkau H, Kulakov AB, Krasnov VM. Superluminal geometrical resonances observed in $Bi_2Sr_2CaCu_2O_{8+x}$ intrinsic Josephson junctions. Phys. Rev. B 82:024517, 2010.
[53] Wang HB, Aruga Y, Tachiki T, Mizugaki Y, Chen J, Nakajima K, Yamashita T, Wu PH. Microwave-induced current steps in intrinsic Josephson junctions patterned on $Bi_2Sr_2CaCu_2O_8$ single crystal. Appl. Phys. Lett. 74:3693, 1999.
[54] Doh Y-J, Kim J, Chang H-S, Chang S, Lee H-J, Kim K-T, Lee W, Choy J-H. Coherent mode splitting of microwave-induced fluxons in HgI_2-intercalated $Bi_2Sr_2CaCu_2O_{8+\delta}$ single crystals. Phys. Rev. B 63:144523, 2001.
[55] Koyama T, Tachiki M. I-V characteristics of Josephson-coupled layered superconductors with longitudinal plasma excitations. Phys. Rev. B 54:16183, 1996.
[56] Matsumoto H, Sakamoto S, Wajima F, Koyama T, Machida M. Simulation of $I - V$ hysteresis branches in an intrinsic stack of Josephson junctions in high-T_c superconductors. Phys. Rev. B 60:3666, 1999.
[57] Sakamoto S, Matsumoto H, Koyama T, Machida M. Voltage-biased $I - V$ characteristics in the multiple Josephson junction model of high-T_c superconductors. Phys. Rev. B 61:3707, 2000.
[58] Shukrinov YuM, Mahfouzi F. Influence of coupling between junctions on breakpoint current in intrinsic Josephson junctions. Phys. Rev. Lett. 98:157001, 2007.
[59] Shukrinov YuM, Mahfouzi F, Pedersen NF. Investigation of the breakpoint region in stacks with a finite number of intrinsic Josephson junctions. Phys. Rev. B 75:104508, 2007.
[60] Shukrinov YuM, Gaafar MA. Charging of superconducting layers and resonance-related hysteresis in the current-voltage characteristics of coupled Josephson junctions. Phys. Rev. B 84:094514, 2011.
[61] Artemenko SN, Kobelkov AG. Intrinsic Josephson effect and violation of the Josephson relation in layered superconductors. Phys. Rev. Lett. 78:3551, 1997.
[62] Ryndyk DA. Collective dynamics of intrinsic Josephson junctions in high- T_c superconductors. Phys. Rev. Lett. 80:3376, 1998.
[63] Preis Ch, Helm Ch, Keller J, Sergeev A, Kleiner R. Coupling of intrinsic Josephson oscillations in layered superconductors by charge fluctuations. Proc. SPIE 3480:236, 1998.
[64] Wang HB, Guénon S, Yuan J, Iishi A, Arisawa S, Hatano T, Yamashita T, Koelle D, Kleiner R. Hot spots and waves in $Bi_2Sr_2CaCu_2O_8$ intrinsic Josephson junction stacks: A study by low temperature scanning laser microscopy. Phys. Rev. Lett. 102:017006, 2009.

[65] Benseman TM, Koshelev AE, Kwok W-K, Welp U, Vlasko-Vlasov VK, Kadowaki K, Minami H, Watanabe C. Direct imaging of hot spots in $Bi_2Sr_2CaCu_2O_{8+\delta}$ mesa terahertz sources. J. Appl. Phys. 113:133902, 2013.

[66] Minami H, Watanabe C, Sato K, Sekimoto S, Yamamoto T, Kashiwagi T, Klemm RA, Kadowaki K. Local SiC photoluminescence evidence of hot spot formation and sub-THz coherent emission from a rectangular $Bi_2Sr_2CaCu_2O_{8+x}$ mesa. Phys. Rev. B 89:054503, 2014.

[67] Benseman TM, Koshelev AE, Vlasko-Vlasov V, Hao Y, Kwok W-K, Welp U, Keiser C, Gross B, Lange M, Koelle D, Kleiner R, Minami H, Watanabe C, Kadowaki K. Current filamentation in large $Bi_2Sr_2CaCu_2O_{8+\delta}$ mesa devices observed via luminescent and scanning laser thermal microscopy. Phys. Rev. Appl. 3:044017, 2015.

[68] Wang HB, Guénon S, Gross B, Yuan J, Jiang ZG, Zhong YY, Gruenzweig M, Iishi A, Wu PH, Hatano T, Koelle D, Kleiner R. Coherent terahertz emission of intrinsic Josephson junction stacks in the hot spot regime. Phys. Rev. Lett. 105:057002, 2010.

[69] Guénon S, Grünzweig M, Gross B, Yuan J, Jiang ZG, Zhong YY, Iishi A, Wu PH, Hatano T, Koelle D, Wang HB, Kleiner R. Interaction of hot spots and THz waves in $Bi_2Sr_2CaCu_2O_8$ intrinsic Josephson junction stacks of various geometry. Phys. Rev. B 82:214506, 2010.

[70] Tsujimoto M, Yamaki K, Deguchi K, Yamamoto T, Kashiwagi T, Minami H, Tachiki M, Kadowaki K. Geometrical resonance conditions for THz radiation from the intrinsic Josephson junctions in $Bi_2Sr_2CaCu_2O_{8+\delta}$. Phys. Rev. Lett. 105:037005, 2010.

[71] Kashiwagi T, Tsujimoto M, Yamamoto T, Minami H, Yamaki K, Delfanzari K, Deguchi K, Orita N, Koike T, Nakayama R, Kitamura T, Sawamura M, Hagino S, Ishida K, Ivancovic K, Asai H, Tachiki M, Klemm RA, Kadowaki K. High temperature superconductor terahertz emitters: Fundamental physics and its applications. J. J. Appl. Phys. 51:010113, 2012.

[72] Kadowaki K, Tsujimoto M, Yamaki K, Yamamoto T, Kashiwagi T, Minami H, Tachiki M, Klemm RA. Evidence for a dual-source mechanism of THz radiation from rectangular mesas of single crystalline $Bi_2Sr_2CaCu_2O_{8+\delta}$ intrinsic Josephson junctions. J. Phys. Soc. Jpn 79:023703, 2010.

[73] Li MY, Yuan J, Kinev N, Li J, Gross B, Guénon S, Ishii A, Hirata K, Hatano T, Koelle D, Kleiner R, Koshelets VP, Wang HB, Wu PH. Linewidth dependence of coherent terahertz emission from $Bi_2Sr_2CaCu_2O_8$ intrinsic Josephson junction stacks in the hot-spot regime. Phys. Rev. B 86:060505(R), 2012.

[74] Lin SZ, Hu X. Phase dynamics in intrinsic Josephson junctions and their electrodynamics. Phys. Rev. B 79:104507, 2009.

[75] Lin S-Z, Hu X. Response and amplification of terahertz electromagnetic waves in intrinsic Josephson junctions of layered high-T_c superconductor. Phys. Rev. B 82:020504, 2010.

[76] Krasnov VM. Terahertz electromagnetic radiation from intrinsic Josephson junctions at zero magnetic field via breather-type self-oscillations. Phys. Rev. B 83:174517, 2011.

[77] Koyama T, Matsumoto H, Machida M, Ota Y. Multi-scale simulation for terahertz wave emission from the intrinsic Josephson junctions. Supercond. Sci. Technol. 24:085007, 2011.

[78] Liu F, Lin SZ, Hu X. Cavity phenomenon and terahertz radiation of a tall stack of intrinsic Josephson junctions wrapped by a dielectric material. Supercond. Sci. Technol. 26:025003, 2013.

[79] Lin SZ, Hu X. In-plane dissipation as a possible synchronization mechanism for terahertz radiation from intrinsic Josephson junctions of layered superconductors. Phys. Rev. B 86:054506, 2012.

[80] Yurgens AA. Temperature distribution in a large $Bi_2Sr_2CaCu_2O_{8+\delta}$ mesa. Phys. Rev. B 83:184501, 2011.

[81] Yurgens AA, Bulaevskii LN. Temperature distribution in a stack of intrinsic Josephson junctions with their CuO-plane electrodes oriented perpendicular to supporting substrate. Supercond. Sci. Technol 24:015003, 2011.

[82] Gross B, Guénon S, Yuan J, Li MY, Li J, Iishi A, Mints RG, Hatano T, Wu PH, Koelle D, Wang HB, Kleiner R. Hot-spot formation in stacks of intrinsic Josephson junctions in $Bi_2Sr_2CaCu_2O_8$. Phys. Rev. B 86:094524, 2012.

[83] Gurevich AV, Mints RG. Self-heating in normal metals and superconductors. Rev. Mod. Phys. 59:941, 1987.

[84] Spenke E. Zur technischen Beherrschung des Wärmedurchschlages von Heissleitern. Wissenschaftliche Veröffentlichungen aus den Siemens-Werken, 15(1):92, 1936.

[85] Asai H, Tachiki M, Kadowaki K. Three-dimensional numerical analysis of terahertz radiation emitted from intrinsic Josephson junctions with hot spots. Phys. Rev. B 85:064521, 2011.

[86] Gross B, Yuan J, An DY, Li MY, Kinev N, Zhou XJ, Ji M, Huang Y, Hatano T, Mints RG, Koshelets VP, Wu PH, Wang HB, Koelle D, Kleiner R. Modeling the linewidth dependence of coherent terahertz emission from intrinsic Josephson junction stacks in the hot-spot regime. Phys. Rev. B 88:014524, 2013.

[87] Rudau F, Tsujimoto M, Gross B, Judd TE, Wieland R, Goldobin E, Kinev N, Yuan J, Huang Y, Ji M, Zhou XJ, An DY, Ishii A, Mints RG, Wu PH, Hatano T, Wang HB, Koshelets VP, Koelle D, Kleiner R. Thermal and electromagnetic properties of $Bi_2Sr_2CaCu_2O_8$ intrinsic Josephson junction stacks studied via one-dimensional coupled sine-Gordon equations. Phys. Rev. B 91:104513, 2015.

[88] Rudau F, Wieland R, Langer J, Zhou XJ, Ji M, Kinev N, Hao LY, Huang Y, Li J, Wu PH, Hatano T, Koshelets VP, Wang HB, Koelle D, Kleiner R. 3D simulations of the electrothermal and THz emission properties of $Bi_2Sr_2CaCu_2O_8$ intrinsic Josephson junction stacks. Phys. Rev. Appl. 5:044017, 2016.

[89] Yuan J, Li MY, Li J, Gross B, Ishii A, Yamaura K, Hatano T, Hirata K, Takayama-Muromachi E, Wu PH, Koelle D, Kleiner R, Wang HB. Terahertz emission from $Bi_2Sr_2CaCu_2O_{8+\delta}$ intrinsic Josephson junction stacks with all-superconducting electrodes. Supercond. Sci. Technol. 25:075015, 2012.

[90] An DY, Yuan J, Kinev N, Li MY, Huang Y, Ji M, Zhang H, Sun ZL, Kang L, Jin BB, Chen J, Li J, Gross B, Ishii A, Hirata K, Hatano T, Koshelets VP, Koelle D, Kleiner R, Wang HB, Xu WW, Wu PH. Terahertz emission and detection both based on high-T_c superconductors: Towards an integrated receiver. Appl. Phys. Lett. 102:092601, 2013.

[91] Sekimoto S, Watanabe C, Minami H, Yamamoto T, Kashiwagi T, Klemm RA, Kadowaki K. Continuous 30 μW terahertz source by a high-T_c superconductor mesa structure. Appl. Phys. Lett. 103:182601, 2013.

[92] Ji M, Yuan J, Gross B, Rudau F, An DY, Li MY, Zhou XJ, Huang Y, Sun HC, Zhu Q, Li J, Kinev N, Hatano T, Koshelets VP, Koelle D, Kleiner R, Xu WW, Jin BB, Wang HB, Wu PH. $Bi_2Sr_2CaCu_2O_8$ intrinsic Josephson junction stacks with improved cooling: Coherent emission above 1 THz. Appl. Phys. Lett. 105:122602, 2014.

[93] Kashiwagi T, Yamamoto T, Kitamura T, Asanuma K, Watanabe C, Nakade K, Yasui T, Saiwai Y, Shibano Y, Kubo H, Sakamoto K, Katsuragawa T, Tsujimoto M, Delfanazari K, Yoshizaki R, Minami H, Klemm RA, Kadowaki K. Generation of electromagnetic waves from 0.3 to 1.6 terahertz with a high-T_c superconducting $Bi_2Sr_2CaCu_2O_{8+\delta}$ intrinsic Josephson junction emitter. Appl. Phys. Lett. 106:092601, 2015.

[94] Sekimoto S, Watanabe C, Minami H, Yamamoto T, Kashiwagi T, Klemm RA, Kadowaki K. Computed tomography image using sub-terahertz waves generated from a high-T_c superconducting intrinsic Josephson junction oscillator. Appl. Phys.Lett. 103:182601, 2013.

[95] Benseman TM, Koshelev AE, Kwok W-K, Welp U, Kadowaki K, Cooper JR, Balakrishnan G. The ac Josephson relation and inhomogeneous temperature distributions in large $Bi_2Sr_2CaCu_2O_{8+\delta}$ mesas for THz emission. Supercond. Sci. Technol. 26:085016, 2013.

[96] Kitamura T, Kashiwagi T, Yamamoto T, Tsujimoto M, Watanabe C, Ishida K, Sekimoto S, Asanuma K, Yasui T, Nakade K, Shibano Y, Saiwai Y, Minami H, Klemm RA, Kadowaki K. Broadly tunable, high-power terahertz radiation up to 73 K from a stand-alone $Bi_2Sr_2CaCu_2O_{8+\delta}$ mesa. Appl. Phys. Lett. 104:202603, 2014.

[97] Kashiwagi T, Yamamoto T, Minami H, Tsujimoto M, Yoshizaki R, Delfanazari K, Kitamura T, Watanabe C, Nakade K, Yasui T, Asanuma K, Saiwai Y, Shibano Y, Enomoto T, Kubo H, Sakamoto K, Katsuragawa T, Marković B, Mirković J, Klemm RA, Kadowaki K. Efficient fabrication of intrinsic-Josephson-junction terahertz oscillators with greatly reduced self-heating effects. Phys. Rev. Applied 4:054018, 2015.

[98] Kashiwagi T, Sakamoto K, Kubo H, Shibano Y, Enomoto T, Kitamura T, Asanuma K, Yasui T, Watanabe C, Nakade K, Saiwai Y, Katsuragawa T, Tsujimoto M, Yoshizaki R, Yamamoto T, Minami H, Klemm RA, Kadowaki K. A high- T_c intrinsic Josephson junction emitter tunable from 0.5 to 2.4 terahertz. Appl. Phys. Lett. 107:082601, 2015.

[99] Benseman TM, Gray KE, Koshelev AE, Kwok W-K, Welp U, Minami H, Kadowaki K, Yamamoto T. Powerful terahertz emission from $Bi_2Sr_2CaCu_2O_{8+\delta}$ mesa arrays. Appl. Phys. Lett. 103:022602, 2013.

[100] Zhou XJ, Zhu Q, Ji M, An DY, Hao LY, Sun HC, Ishida S, Rudau F, Wieland R, Li J, Koelle D, Eisaki H, Yoshida Y, Hatano T, Kleiner R, Wang HB, Wu PH. Three-terminal stand-alone superconducting terahertz emitter. Appl. Phys. Lett. 107:122602, 2015.

[101] Watanabe C, Minami H, Kitamura T, Asanuma K, Nakade K, Yasui T, Saiwai Y, Shibano Y, Yamamoto T, Kashiwagi T, Klemm RA, Kadowaki K. Influence of the local heating position on the terahertz emission power from high-T_c superconducting $Bi_2Sr_2CaCu_2O_{8+\delta}$ mesas. Appl. Phys. Lett. 106:042603, 2015.

[102] Zhou XJ, Yuan J, Wu H, Gao ZS, Ji M, An DY, Huang Y, Rudau F, Wieland R, Gross B, Kinev N, Li J, Ishii A, Hatano T, Koshelets VP, Koelle D, Kleiner R, Wang HB, Wu PH. Tuning the terahertz emission power of an intrinsic Josephson-junction stack with a focused laser beam. Phys. Rev. Applied 3:044012, 2015.

[103] Kashiwagi T, Nakade K, Markovic B, Saiwai Y, Minami H, Kitamura T, Watanabe C, Ishida K, Sekimoto S, Asanuma K, Yasui T, Shibano Y, Tsujimoto M, Yamamoto T, Mirkovic J, Kadowaki K. Reflection type of terahertz imaging system using a high-T_c superconducting oscillator. Appl. Phys. Lett. 104:022601, 2014.

[104] Tsujimoto M, Minami H, Delfanazari K, Sawamura M, Nakayama R, Kitamura T, Yamamoto T, Kashiwagi T, Hattori T, and Kadowaki K, Terahertz imaging system using high-T_c superconducting oscillation devices. Appl J. Phys. 111:123111, 2012.

[105] Kashiwagi T, Nakade K, Saiwai Y, Minami H, Kitamura T, Watanabe C, Ishida K, Sekimoto S, Asanuma K, Yasui T, Shibano Y, Tsujimoto M, Yamamoto T, Markovic B, Mirkovic J, Klemm RA, Kadowaki K. Computed tomography image using sub-terahertz waves generated from a high-T_c superconducting intrinsic Josephson junction oscillator. Appl. Phys. Lett. 104:082603, 2014.

[106] Hao LY, Ji M, Yuan J, An DY, Li MY, Zhou XJ, Huang Y, Sun HC, Zhu Q, Rudau F, Wieland R, Kinev N, Li J, Xu WW, Jin BB, Chen J, Hatano T, Koshelets VP, Koelle D, Kleiner R, Wang HB, Wu PH. Compact superconducting terahertz source operating in liquid nitrogen. Phys. Rev. Appl. 3:024006, 2015.